Modelling semiflexible polymers: shape analysis, buckling instabilities, and force generation†‡

Jan Kierfeld,*[ab] Krzysztof Baczynski,[a] Petra Gutjahr,[a] Torsten Kühne[a] and Reinhard Lipowsky[a]

The behavior of semiflexible polymers and filaments is governed by their bending energy. The corresponding bending rigidity gives rise to material properties that are distinct from those of flexible polymers governed by entropy. In particular, bending rigidity plays an important role for the shapes of these polymers and their ability to withstand and transmit forces. Recent theoretical studies and modelling approaches are briefly reviewed and used for a systematic analysis of shapes of adsorbed semiflexible polymers and buckling instabilities. Semiflexible polymers and filaments exhibit a buckling instability which is modified by thermal fluctuations and provides upper bounds on the generation of polymerization forces. Growing bundles of polymers or filaments can generate force *via* adhesive interactions. The latter mechanism remains effective even after single filaments have attained a buckled state.

1 Introduction

The properties of typical synthetic polymers such as polyethylene are governed by entropic elasticity and excluded volume interactions. These polymers deform easily and enthalpic contributions to their elasticity are small.[1] Semiflexible polymers, on the other hand, are stiff polymers with a considerable bending energy. The material parameter characterizing the bending energy is the bending rigidity κ. The competition between bending energy and thermal fluctuations determines a characteristic length scale, the persistence length $L_p = \kappa/k_BT$. On length scales smaller than the persistence length, the bending energy is more relevant than entropic elasticity. For a freely fluctuating semiflexible polymer the persistence length is the decay length of orientation correlations,[2,3] *i.e.*, the typical length scale over which a thermally fluctuating semiflexible polymer changes its orientation. Semiflexible polymers show interesting material properties if the persistence length exceeds other relevant length scales such as the contour length L of the polymer. Then their behavior becomes dominated by bending energy rather than entropy.

Polymer chemistry and biology provide a number of examples of semiflexible polymers, whose persistence length is comparable to typical contour lengths. Most of the following examples are supramolecular assemblies with a rather large diameter which gives rise to strong interactions along their backbone and results in a large resistance to bending. Important examples from cell biology are filaments of the cytoskeleton such as filamentous actin (F-actin) with a persistence length around 10 μm[4,5] and microtubules with persistence lengths of several mm.[5] Because of their bending rigidity, these filaments play an important role in the mechanical stability of the cytoskeleton. Likewise, DNA is a semiflexible polymer with a mechanical persistence length of 50 nm.[6] Polymer chemistry provides various examples of synthetic semiflexible polymers. Polyelectrolytes at low salt concentrations stiffen because of repulsive Coulomb interactions, which leads to a persistence length determined by the charge density along the polymer backbone and the salt concentration of the surrounding solution.[7] Dendronized polymers[8] are stiff because of steric interaction between their dendritic side groups. metallosupramolecular coordination polyelectrolytes (MEPE) self-assemble from metallic ions and suitable ligands into rather stiff rods.[9,10] Finally, carbon nanotubes are examples of extremely stiff synthetic rods built from covalently bonded carbon sheets with persistence lengths around 1 μm.[11]

The bending rigidity κ can be determined experimentally by analyzing thermal shape fluctuations of freely fluctuating semiflexible polymers as in ref. 4 and 5 to measure the persistence length of cytoskeletal filaments, or by analyzing thermal shape fluctuations in confining channels.[12] Another way of measuring persistence length is to determine ring closure probabilities of semiflexible rings.[6,11] Here, we propose a method based on theoretical results for equilibrium shapes of semiflexible polymer rings adsorbed to a substrate containing a stripe structure. Based on these results the bending rigidity could be determined from observed sequences of distinct equilibrium ring shapes that are induced by the substrate structure.

Stiff polymers are also more stable with respect to the classical Euler buckling instability,[13] which limits the compressive force that a rod of bending rigidity κ can sustain without buckling to the critical Euler buckling force $F_c \propto \kappa/L^2$. Cytoskeletal filaments give the cell structural stability because of this resistance to compressive forces. Typical buckling forces of cytoskeletal filaments are in the pico-newton range and, thus, comparable to thermal forces on the nanometre scale. Therefore, it is important

[a] Max Planck Institute of Colloids and Interfaces, Science Park Golm, 14424 Potsdam, Germany. E-mail: Jan.Kierfeld@tu-dortmund.de
[b] Physics Department, TU Dortmund University, 44221 Dortmund, Germany

† This paper is part of a *Soft Matter* themed issue on The Physics of Buckling. Guest editor: Alfred Crosby.

to model the influence of thermal fluctuations on the buckling instability.

Filaments do not only serve as structural elements of the cytoskeleton but are actively involved in force generation in cell motility and cell division. Polymerization of single cytoskeletal filaments can generate forces in the pico-newton range, which are used to push the lamellipodium of moving cells. The transmission of these forces is limited by the buckling instability. We will present a theoretical model for a simple mechanism of force generation by semiflexible polymer bundles, which is not limited by the buckling instability of single polymers but relies on adhesive interactions between polymers. This mechanism could be used to generate forces by synthetic polymers as well.

2 Shape analysis

Bionanotechnology requires the immobilization and controlled manipulation of DNA and other semiflexible polymers. Adsorption is the simplest technique to immobilize single polymers and a first step towards further visualization and manipulation using, e.g., modern scanning probe techniques.[14,15] For manipulation, control over the shape of the adsorbed polymer is needed. We show by theoretical modelling that for semiflexible polymer rings such shape control can be achieved using relatively simple surface structures with a stripe geometry, which can be realized by topographical or chemical structuring. Topographical surface steps have been employed in recent manipulation experiments on semiflexible polymer rings.[16] Whereas flexible polymers are governed by conformational entropy and typically adsorb in random coil configurations, the morphologies of semiflexible polymers with large persistence lengths are dominated by their bending rigidity: on a homogeneous adsorbing substrate, an open polymer adsorbs in a straight configuration, whereas a closed polymer ring forms a circular loop. Examples of such semiflexible loops are provided by DNA minicircles,[17] carbon nanotubes,[11] and filamentous actin.[18]

Here we consider the presence of an additional adhesive surface structure with a stripe geometry, which can be either a topographical surface groove with rectangular cross section,

see Fig. 1(a), or a striped domain of increased adhesion energy, see Fig. 1(b), to introduce a laterally modulated adhesion potential, which tends to confine the ring to the stripe.

The shapes of a semiflexible ring adsorbed to a striped surface geometry are governed by two competing energies: the adsorption energy E_{ad} determined by the striped surface structure and the bending energy E_b of the closed polymer ring. The bending energy of a semiflexible polymer of contour length L is given by

$$E_b = \frac{\kappa}{2}\int_0^L ds(\partial_s \mathbf{t})^2 = \frac{\kappa}{2}\int_0^L ds(\partial_s \phi(s))^2 \qquad (1)$$

where κ is the bending rigidity, s is the arc length with $0 < s < L$, ∂_s indicates a derivative with respect to s, and $\mathbf{t}(s)$ is the unit tangent. For a planar polymer we can fulfil the constraint $|\mathbf{t}(s)| = 1$ explicitly by using a parametrization in terms of the tangent angle $\phi(s)$, i.e., $\mathbf{t}(s) = (\cos \phi(s), \sin \phi(s))$ leading to the second equality. The adsorption energy profile resulting from a topographical stripe consists of two adhesive lines at the corners of the rectangular groove of width a_{st}, where the polymer can bind to two adjacent surfaces as shown in Fig. 1(a). Therefore, the adsorption energy is given by $E_{ad} = -|W_{st}|L_{st}$, where L_{st} is the length of the straight adhered segments on the corners of the rectangular groove and $W_{st} < 0$ the additional adsorption energy per polymer length at the corner of the groove, where it can bind to two adjacent surfaces. For a chemical surface domain, on the other hand, the adsorption energy is increased over the whole area of the stripe of width a_{do}, see Fig. 1(b). Therefore, the adsorption energy is given by $E_{ad} = -|W_{do}|L_{do}$, where L_{do} is given by the polymer length within the whole area of the stripe domain, and $W_{do} < 0$ the additional adsorption energy per polymer length in the stripe domain.

The contour length L of the polymer ring and the width of the stripe structure are the relevant geometric control parameters, which can be combined into a reduced contour length L/a_{st} or L/a_{do}. The energetic control parameters are the bending rigidity κ of the semiflexible polymer and the strength W_{st} or W_{do} of the additional adsorption potential in the stripe structure. These energies can be combined to a single reduced adhesion strength $w_{st} = W_{st}a_{st}^2/\kappa$ or $w_{do} = W_{do}a_{do}^2/\kappa$. We find that we can completely classify the possible stable morphologies and shape transitions between these morphologies using only two parameters, the reduced contour length and the reduced adhesion strength.

Stable morphologies can be identified by minimizing the total energy of the polymer ring, $E_{tot} = E_{ad} + E_b$ under the constraints imposed by ring closure. The bending energy prefers a round shape and the adhesion energy prefers an elongated shape in the stripe geometry. We performed this energy minimization both numerically using the dynamical discretization algorithm provided by the SURFACE EVOLVER[19] and by approximate analytical techniques. Here we present the main results. Using this combination of techniques we find for both types of stripe structures that the semiflexible polymer ring displays up to four stable morphologies, which are shown in Fig. 1. We can switch between these four stable morphologies by changing one of the control parameters, for example by changing the adhesion contrast or the polymer length. For small reduced adhesion strength the ring assumes a round toroidal shape I. Upon increasing the adhesion of the stripe, this shape becomes unstable with respect to the elongated configurations of type II, which can
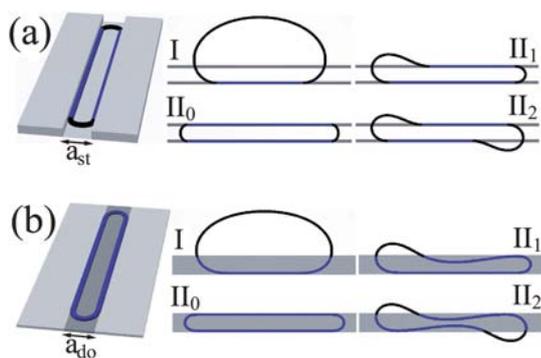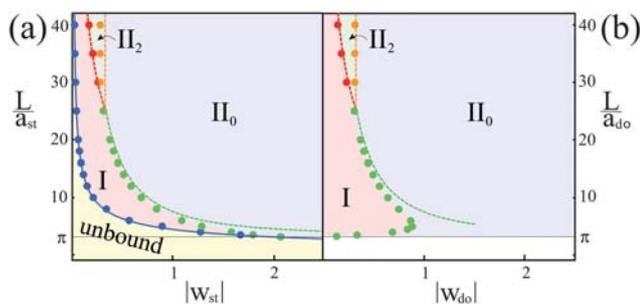

Fig. 1 The adsorbed polymer on a striped surface containing (a) two topographical surface steps forming a rectangular groove of width a_{st} and (b) a chemically structured surface domain of width a_{do}. Top views of all four stable ring morphologies as obtained by energy minimization for contour lengths $L/a_{st} = 20$ and $L/a_{do} = 20$. The corresponding oblique views show the surface topography and the chemical surface domain with an elongated shape II_0.

display additional bulges at their ends. According to the number of bulges we call these configurations II_0, II_1, or II_2 as shown in Fig. 1.

A systematic comparison of the total energies of all four possible metastable states for given reduced contour length and given reduced adhesion strength allows us to determine the globally stable state, which is given by the shape with the smallest total energy. As a function of the two control parameters, reduced adhesion strength and reduced contour length, we can obtain a complete classification of the stability of these shapes, which leads to the morphology diagrams in Fig. 2. In these diagrams we show which of the shapes is globally stable in a given parameter region. The diagrams also show good agreement between the approximate analytical results, which give the lines indicating transitions between different shapes, and the exact numerical minimization results, which are shown as data points. It is remarkable that the topographical and chemical stripes give rise to qualitatively very similar morphology diagrams Fig. 2(a) and (b), respectively. Both types of structures lead to very similar behavior with a *discontinuous morphological transition* between the two dominant shapes I and II_0, with intermediate bulged shape II_2 for large contour lengths. The morphology diagrams in Fig. 2 also show that the state II_1 with a single bulge is the most metastable. The main difference between the topographical and chemical stripe is the existence of an unbound ring state for the topographical groove, where the polymer ring prefers to completely detach from the corner of the groove and assume a circular shape.[20]

By means of a morphology diagram as obtained in Fig. 2 by theoretical modelling, protocols for controlled switching between the different ring shapes can be predicted. An increase in the adhesion contrast, for example, corresponds to a horizontal trajectory in the diagram, which should result in transitions from a round state I to an elongated state II_0 with an eventual intermediate state II_2 with two bulges. Furthermore, observed sequences of shapes upon changing parameters like the adhesion contrast can be used to infer material parameters such as the bending rigidity from the morphology diagram.

Additional control over the shape of semiflexible polymers can be achieved by condensing agents, which introduce attractive interactions between polymer segments.[21,22] For semiflexible

polymers this can induce additional shape transitions into more compact condensed shapes.
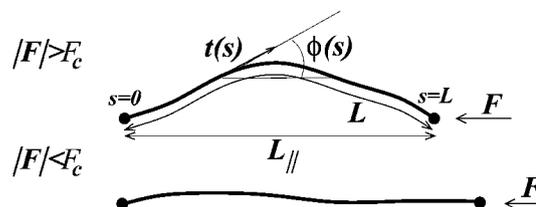
3 Buckling instability

Since the work of Euler, it is well known that a macroscopic rod of length L and bending rigidity κ buckles under a compressive force F which exceeds a critical threshold force $F_c \propto \kappa/L^2$. This is the classical Euler buckling instability in the absence of thermal fluctuations. Semiflexible polymers such as DNA or cytoskeletal filaments can be modelled as elastic rods with a diameter in the nanometre range. Such nanorods have bending rigidities that are small compared to a macroscopic elastic rod, but lead to bending energies that are still larger than the thermal energy for the bending modes on the scale of the polymer contour length, which are most relevant for buckling. Therefore, semiflexible polymers can also undergo a buckling instability, but their bending rigidities are so small that effects arising from thermal fluctuations have to be taken into account. The Euler buckling instability is strongly modified by thermal fluctuations if the persistence length L_p becomes comparable or even smaller than the polymer contour length L.[23–25] For charged polymers the buckling instability is related to the collapse of a stiff polyelectrolyte under the action of attractive intra-chain interactions, which has also been analyzed in the presence of thermal fluctuations.[26]

In ref. 23 we developed a theoretical model of the buckling instability in the presence of thermal fluctuations. In two spatial dimensions we start from a Hamiltonian

$$\mathscr{H} = \int_0^L ds \left[\frac{\kappa}{2}(\partial_s \phi)^2 + F\cos\phi(s) \right], \qquad (2)$$

where $F \equiv |\mathbf{F}|$ is the absolute value of the compressive force, which is acting in the direction $\phi = \pi$, see Fig. 3. The buckling instability is an instability of the bending mode with the longest wavelength which is admissible by the boundary conditions at the ends of the semiflexible polymer. This wavelength is of the order of the contour length of the polymer. By integrating out short-wavelength fluctuations we obtain an effective theory for the longest wavelength mode governing the buckling instability. Our analytical results are corroborated by Monte Carlo computer simulations.

In two spatial dimensions this allows us to calculate the resulting shift of the critical force by fluctuation effects. We find

Fig. 2 Morphology diagrams for (a) the topographical surface groove and (b) the striped chemical surface domain as a function of the reduced contour lengths L/a_{st} and L/a_{do} and the reduced potential strengths $|w_{st}|$ and $|w_{do}|$, respectively. Morphological transitions as obtained from numerical energy minimization are represented by colored dots. The colored lines show the analytical results for the transition lines.

Fig. 3 A thermally fluctuating filament under a compressive force F (for free boundary conditions). For absolute values $|F|$ of the force that exceed the critical buckling force F_c, the filament is buckled; for $|F| < F_c$, the filament remains unbuckled. The filament has a contour length of L, $\mathbf{t}(s)$ is the unit tangent vector, and $\phi(s)$ the corresponding tangent angle at arc length s. The projected length $L_\parallel$ provides an order parameter for buckling.

that the critical force F_c is *increased* by thermal fluctuations in two spatial dimensions,

$$F_c(T) - F_c(0) \propto \frac{k_B T}{L}. \tag{3}$$

This result seems counterintuitive because we expect that small thermal forces should, in general, help in triggering buckling. The threshold force increases because the energy gain by deforming a filament with a force decreases if the filament has already shortened by thermal fluctuations. More sophisticated theoretical arguments suggest that a critical force F_c increased by thermal fluctuations should be found for all spatial dimensions smaller than three.

The mean projected length $\langle L_\parallel \rangle = \int_0^t ds \langle \cos\phi(s) \rangle$ in the direction of the compressive force can be used to construct an order parameter for the buckling instability. After buckling, the projected length shows a linear decrease from the full contour length with increasing compressive force. Thermal fluctuations lead to a rounding of this onset of length decrease, see Fig. 4. Furthermore, we find the following surprising behavior of the mean projected length in the presence of thermal fluctuations: before buckling thermal fluctuations tend to shorten the projected length, reflecting the fact that contour length is pulled into shape undulations of the polymer. After buckling, on the other hand, thermal fluctuations tend to stretch the semiflexible polymer, *i.e.*, its mean projected length in the direction of the applied force increases by thermal fluctuations. This gives rise to intersecting force extension curves in Fig. 4, which signal the transition from an *entropic* spring behavior with an effective spring constant that increases upon heating for forces smaller than the buckling force, to an *enthalpic* behavior with an effective spring constant that decreases upon heating for forces larger than the buckling force.

These results show that thermally fluctuating semiflexible polymers exhibit a buckling instability analogous to the mechanical Euler instability in the absence of thermal fluctuations. Thermal fluctuations lead to significant modifications of this instability and stretch a semiflexible polymer in its buckled state while they shorten it in the unbuckled state.
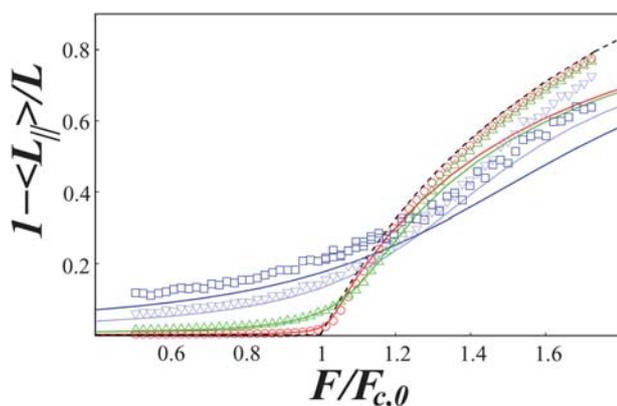
Fig. 4 The reduced mean projected length $1-\langle L_\parallel \rangle/L$ as a function of the applied compressive force F/F_c at fixed contour length L. Different colors indicate different ratios L_p/L of persistence length to contour length. For decreasing ratios L_p/L (from red to blue) thermal fluctuations increase. The solid lines are analytical results,[23] the data points are from Monte-Carlo simulations.

4 Force generation and buckling

In the context of biological systems, it has been shown that single polymerizing filaments can generate forces in the pico-newton range by converting the polymerization energy associated with monomer addition into force.[27] For single filaments, this has been experimentally demonstrated for the first time by analyzing shapes of buckling microtubules growing against a fixed obstacle.[28] Several ratchet models have been proposed to model the dynamics of this process.[29,30] In order to quantify force generation, we consider the polymerization of a semiflexible polymer against a perpendicular rigid planar wall onto which the polymerization force is transmitted. If the wall is loaded by an additional force F, polymerization is slowed down because the rate for monomer addition is exponentially decreasing under the load force F according to Bell theory.[31] The characteristic force $F = F_p$, which is required to stop the growth process, is identified with the maximal polymerization force that the filament can exert onto the wall.

Such force generation is always limited by the buckling instability, which has been discussed in the previous section: if the generated polymerization force exceeds the critical buckling force, the filament will buckle in front of the wall as shown in Fig. 5. We have shown that single polymerizing filaments will remain in a buckled state after they go through a buckling instability by increasing their length. After buckling, the filament end is no longer perpendicular to the wall. This leads to a reduction of the force component resisting further polymerization such that further growth and buckling will proceed until a fully buckled configuration as shown in Fig. 5 is reached.

Therefore, we study the force-generating mechanism which can also operate if filaments are in the buckled state. In these mechanisms we focus on bundles of semiflexible polymers, which form because of additional attractive interactions between the polymers.[32] Besides the polymerization energy, the attractive interaction energy can provide an additional source of energy which can eventually be converted into force. This leads to a novel zipping mechanism for force-generation, see Fig. 6, which is insensitive to buckling instabilities.[33]

The zipping mechanism is operating for semiflexible polymers in their fully buckled state in a "zipping fork" configuration, where the bundled filaments are in a splayed configuration in
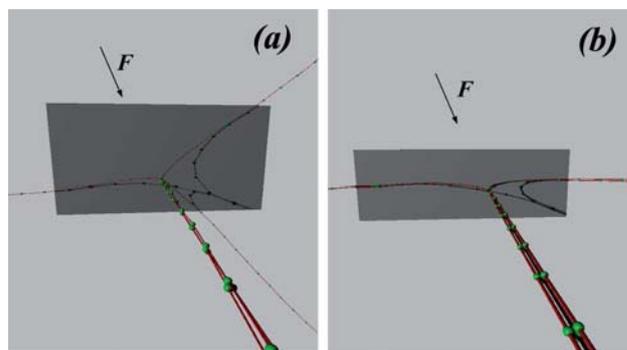
Fig. 5 Snapshots of MC simulations for $N = 3$ filaments in front of a wall under a load force F close to the transition between zipping and force-induced unbinding for two different initial conditions.
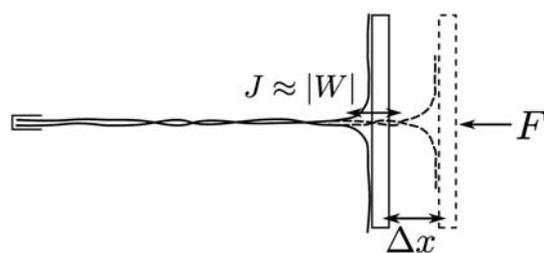
Fig. 6 The zipping mechanism in front of a wall with load force F. Zipping starts in a splayed configuration of filament ends (——). The curvature at the wall is given by the contact radius R_{co}. Zipping a distance Δx (---) performs work $F\Delta x$ but gains an adhesive energy $J\Delta x$, where J is the binding free energy per length.

front the wall, as shown in Fig. 6 or in the simulation snapshots in Fig. 5. We explain the mechanism for two polymers as shown in Fig. 6. In the fully buckled configuration, no force is transmitted onto the wall upon further polymerization at the polymer ends because the end segments are oriented parallel to the wall. However, if both polymers further zip together along an additional length Δx, the bundle lowers its free energy by an amount $J\Delta x$, where $J > 0$ is the binding free energy (per length). This binding free energy arises from a short-range attraction between filaments, which competes with thermal shape fluctuations of filaments.[32] The potential strength of this short-range attraction is denoted by W in the following. If the polymers zip together, the wall has to move as well by a distance Δx against the external load force F. This movement requires mechanical work $F\Delta x$ such that the total free energy of the bundle changes by $(F–J)\Delta x$. This means that zipping will occur if the binding free energy J exceeds the load force F such that the total free energy of the bundle is lowered by zipping. If J is smaller than F the reverse process of

force-induced unbinding will take place, and the bundle is further split apart.

The zipping mechanism requires a certain bending rigidity of the semiflexible polymers. This bending rigidity has to ensure that the zipped bundle is stable against buckling at the applied force F. Furthermore, the bending rigidity is important in order to transmit force onto the wall in the fully buckled state.

In order to gain further quantitative insight into this zipping mechanism we performed kinetic Monte Carlo simulations on bundles with $N \geq 2$ filaments. In the MC simulation we use for each filament a discretized representation of the bending energy (1) and model the constraint $|\mathbf{t}(s)| = 1$ by a sufficiently stiff harmonic potential. We include additional pairwise attractive interactions between segments on different filaments, which are also discretized in the coordinate s along the filaments. The interactions contain a hard core and a short-range attraction.[32] In addition we allow attachment and detachment of monomers, which lead to a change of the contour length. The ratio of attachment and detachment rate is determined by a polymerization energy. The attachment rate is exponentially decreased with mechanical work $F\Delta x$ performed by monomer attachment according to Bell theory.[31] Snapshots from these simulations for $N = 3$ filaments are shown in Fig. 5. In the Monte Carlo simulations, we can demonstrate the zipping mechanism or the reverse mechanism of force-induced unbinding and show that the force-induced unbinding transition occurs (i) in several steps, (ii) at critical potential strengths, which depend on the load force, and (iii) via different pathways depending on the initial sub-bundle configuration. The number of transition steps and the critical potential strengths in force-induced unbinding depend on the initial zipping fork configuration, in particular on the number and types of sub-bundles in the initial splayed configuration. These findings are summarized in Fig. 7, where the polymer
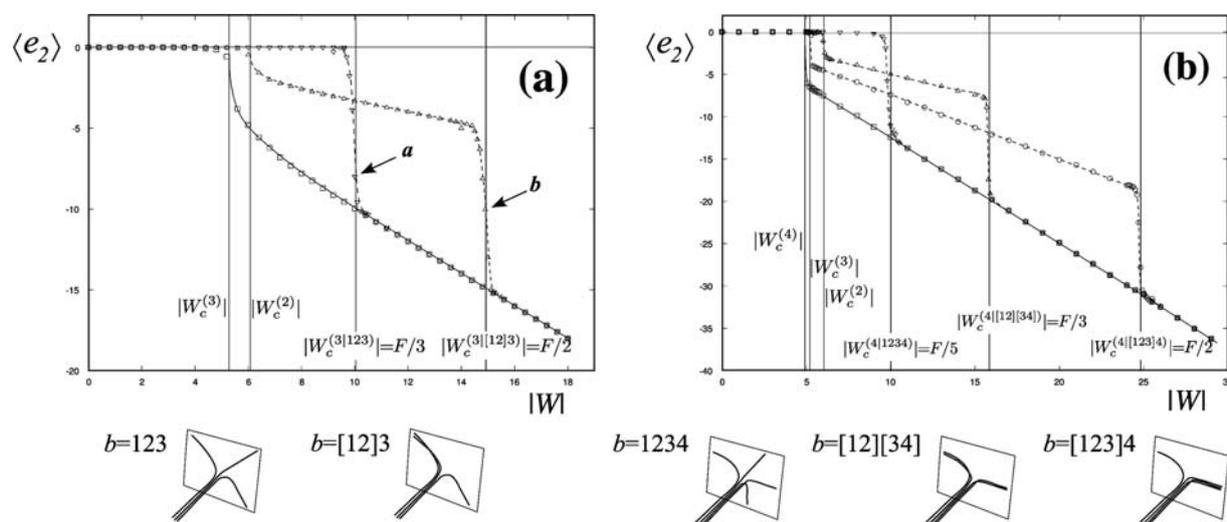
Fig. 7 Monte Carlo data for the average interaction energy per filament and per length, $\langle e_2 \rangle$, as a function of the potential strength $|W|$ for (a) $N = 3$ and (b) $N = 4$ identical filaments. Arrows correspond to the snapshots in Fig. 5. In the absence of an external force $F = 0$ ($\square$), the thermal unbinding transition happens at a critical potential strength $|W_c^{(N)}|$. (a) For $N = 3$ an external force $F = 30$ is applied. For an initial configuration $b = 123$ ($\triangledown$), the unbinding transition occurs at a critical potential strength $|W_c^{(3|123)}| \approx F/3$. For an initial condition $b = [12]3$ ($\triangle$), a cascade of two unbinding transition occurs at critical potential strengths $|W_c^{(2)}|$ and $|W_c^{(3|[12]3)}| \approx F/2$. (b) For $N = 4$ filaments an external force $F = 50$ is applied. This leads to three different force-dependent critical potential strengths $|W_c^{(4|1234)}| \approx F/5$ ($\triangledown$), $|W_c^{(4|[123]4)}| \approx F/3$ ($\bigcirc$), and $|W_c^{(4|[12][34])}| \approx F/2$ ($\triangle$) depending on the initial sub-bundle configuration.

binding energy is shown for different unbinding pathways, *i.e.*, upon reducing the potential strength $|W|$ in the presence of a loading force. Discontinuous jumps in the binding energy represent discontinuous force-induced unbinding transitions.

For a bundle with $N = 3$ filaments, two different initial zipping fork configurations and, thus, two force-induced unbinding pathways are possible, see Fig. 7(a). In configuration $b = 123$, all three filaments point in different directions. In configuration $b = [12]3$, the end of the bundle is split into one sub-bundle of two bound filaments [12] and the third filament 3 pointing in a different direction. In configuration $b = 123$ all three filaments point in different directions, and there is a single unbinding transition at $|W^{(3|123)}_c| \approx F/3$ because three pairwise filament interactions are lost upon unbinding. In configuration $b = [12]3$, on the other hand, there is a cascade of two unbinding transitions: first, filament 3 is separated from the sub-bundle [12] at a potential strength $|W^{(3|123)}_c| \approx F/2$ because two pairwise filament interactions are lost upon sub-bundle unbinding. Further decreasing the potential strength $|W|$, there is a second thermal unbinding transition of the sub-bundle [12] at the critical value $|W^{(2)}_c|$, which is independent of force. For $N = 4$ filaments even more unbinding pathways are possible as shown in Fig. 7(b).

The zipping forces which can be created by this mechanism are given by the adhesion energy per length between the semiflexible polymers. For biological filaments, adhesion energies can be generated by crosslinking proteins, for synthetic polymers electrostatic interactions can give rise to adhesion. If adhesion energies of the order of $k_B T$ can be generated per nanometre and per filament pair, the resulting zipping forces are in the pico-newton range already for small bundles containing only two filaments. They easily reach tens of pico-newtons for larger bundles.

The zipping mechanism is conceptually simple and only relies on adhesive energy. With respect to biological systems and cell biology such a mechanism might be realized in relatively primitive cells. For example, a very similar mechanism has been proposed to play a role for the motility of sperm cells of nematodes.[34] Zipping mechanisms could also be exploited to create artificial force generating systems using synthetic semiflexible polymers with attractive interactions.

5 Conclusion

The results presented show that theoretical modelling approaches and simulations are useful tools in analyzing material properties and the possible applications of stiff semiflexible polymers. Modelling approaches are helpful in designing potential experiments to measure important material parameters such as the bending rigidity. This has been demonstrated by a systematic theoretical analysis of shapes of semiflexible polymer rings on substrates with striped surface structures, which could be used to interpret experimentally observed shape sequences. We also discussed how simulations allow the demonstration of interesting applications of semiflexible

polymers such as the force generation by growing polymer bundles based on a zipping mechanism.

6 Acknowledgements

References

1 M. Doi and S. Edwards, *The Theory of Polymer Dynamics*, Oxford University Press, Oxford, 1986.
2 O. Kratky and G. Porod, *Recl. Trav. Chim. Pays-Bas*, 1949, **68**, 1106–1122.
3 E. Lifshitz and L. Landau, *Statistical Physics, Part 1*, Pergamon Press, New York, 1969.
4 J. Käs, H. Strey and E. Sackmann, *Nature*, 1994, **368**, 226–229.
5 F. Gittes, B. Mickey, J. Nettleton and J. Howard, *J. Mol. Biol.*, 1993, **120**, 923–934.
6 W. Taylor and P. Hagerman, *J. Mol. Biol.*, 1990, **212**, 363–376.
7 J.-L. Barrat and J.-F. Joanny, *Advances in Chemical Physics, Vol. XCIV*, John Wiley & Sons, New York, 1996.
8 A. Schlüter and J. Rabe, *Angew. Chem., Int. Ed.*, 2000, **39**, 864–883.
9 M. Schütte, D. Kurth, M. Linford, H. Cölfen and H. Möhwald, *Angew. Chem., Int. Ed.*, 1998, **37**, 2891–2893.
10 D. Kurth, N. Severin and J. Rabe, *Angew. Chem., Int. Ed.*, 2002, **41**, 3681–3683.
11 M. Sano, A. Kamino, J. Okamura and S. Shinkai, *Science*, 2001, **293**, 1299–1301.
12 S. Köster, J. Kierfeld and T. Pfohl, *Eur. Phys. J. E*, 2008, **25**, 439–449.
13 E. Lifshitz and L. Landau, *Theory of Elasticity*, Pergamon Press, New York, 1986.
14 S. Sheiko and M. Möller, *Chem. Rev.*, 2001, **101**, 4099–4123.
15 P. Samori, *J. Mater. Chem.*, 2004, **14**, 1353–1366.
16 N. Severin, W. Zhuang, C. Ecker, A. Kalachev, I. Sokolov and J. Rabe, *Nano Lett.*, 2006, **6**, 2561–2566.
17 A. Amzallag, C. Vaillant, M. Jacob, M. Unser, J. Bednar, J. Kahn, J. Dubochet, A. Stasiak and J. Maddocks, *Nucleic Acids Res.*, 2006, **34**, e125.
18 J. Tang, J. Käs, J. Shah and P. Janmey, *Eur. Biophys. J.*, 2001, **30**, 477–484.
19 K. Brakke, *Exp. Math.*, 1992, **1**, 141–165.
20 U. Seifert and R. Lipowsky, *Phys. Rev. A: At., Mol., Opt. Phys.*, 1990, **42**, 4768–4771.
21 V. Bloomfield, *Biopolymers*, 1997, **44**, 269–282.
22 C. Zhang, P. Shao, J. van Kan and J. van der Maarel, *Proc. Natl. Acad. Sci. U. S. A.*, 2009, **106**, 16651–16656.
23 K. Baczynski, R. Lipowsky and J. Kierfeld, *Phys. Rev. E: Stat., Nonlinear, Soft Matter Phys.*, 2007, **76**, 061914.
24 M. Emanuel, H. Mohrbach, M. Sayar, H. Schiessel and I. Kulic, *Phys. Rev. E: Stat., Nonlinear, Soft Matter Phys.*, 2007, **76**, 061907.
25 N.-K. Lee, A. Johner and S.-C. Hong, *Eur. Phys. J. E*, 2007, **24**, 229–241.
26 P. Hansen, D. Svensek, V. Parsegian and R. Podgornik, *Phys. Rev. E: Stat. Phys., Plasmas, Fluids, Relat. Interdiscip. Top.*, 1999, **60**, 1956–1966.
27 J. Theriot, *Traffic*, 2000, **1**, 19–28.
28 M. Dogterom and B. Yurke, *Science*, 1997, **278**, 856–860.
29 C. Peskin, G. M. Odell and G. F. Oster, *Biophys. J.*, 1993, **65**, 316–324.
30 A. Mogilner and G. Oster, *Biophys. J.*, 1996, **71**, 3030–3045.
31 G. Bell, *Science*, 1978, **200**, 618–627.
32 J. Kierfeld, T. Kühne and R. Lipowsky, *Phys. Rev. Lett.*, 2005, **95**, 038102.
33 T. Kühne, R. Lipowsky and J. Kierfeld, *Europhys. Lett.*, 2009, **86**, 68002.
34 A. Mogilner and G. Oster, *Science*, 2003, **302**, 1340–1341.